

Hierarchical porous Nickel Cobaltate Nanotube as Electrocatalyst for Lithium-Oxygen Batteries

Xiang Chen^{†,1}, Peng Kuang^{†,3}, Chunguang Chen², Xiuhui Zhang², Tao Huang^{1,*}, Lijuan Zhang^{1,*}, Aishui Yu^{1,2,*}

¹ Laboratory of Advanced Materials, Shanghai Key Laboratory of Molecular Catalysis and Innovative Materials, Institute of New Energy, Collaborative Innovation Center of Chemistry for Energy Materials, Fudan University, Shanghai 200433, China.

² Department of Chemistry, Shanghai Key Laboratory of Molecular Catalysis and Innovative Materials, Institute of New Energy, Collaborative Innovation Center of Chemistry for Energy Materials, Fudan University, Shanghai 200433, China.

³ Division II, BYD Company Limited. No.999 Xiang Jing Road, Songjiang District, Shanghai, China

*E-mail: asyu@fudan.edu.cn

† The two authors contributed equally to this work.

Received: 3 January 2018 / Accepted: 8 February 2018 / Published: 6 March 2018

Binary metal oxides are considered as effective catalysts owing to their excellent oxygen evolution reaction (OER) and oxygen reduction reaction (ORR) activity. In this report, NiCo₂O₄ nanotube with hierarchical porous structure is synthesized through a hydrothermal method and following annealing. Scanning electron microscopy (SEM) and transmission electron microscopy (TEM) show its morphology of nanotube and subunit of nanoflake. BET N₂ adsorption-desorption test shows a high specific surface area of 129.03 m² g⁻¹ and hierarchical pores ranging 2-5 nm. When used as lithium-oxygen batteries electrocatalyst, it evidently reduces overpotential (2.64/3.92 V) and improves the specific capacity (1979 mAh g⁻¹) and cycle life (42 cycles) of the cell.

Keywords: lithium-oxygen batteries, porous structure, nanotube, binary metal oxides

1. INTRODUCTION

Lithium-oxygen battery has gained much attention from new energy storage researchers worldwide because of its high theoretical energy density (5200 Wh kg⁻¹)[1]. However, its practical application is hindered by low power density, energy efficiency, short cycle life[2, 3]. A proper bifunctional electrocatalyst is a key to these problems[4, 5]. Carbon material including graphene[6], nanotube[7], carbon nanofiber[8], carbon spheres[9] have been widely investigated. Because of high

electron conducting ability, hierarchical pore structure and low density, many carbon materials show outstanding specific capacity and high charge overpotential. In a carbon-based lithium-oxygen battery, discharge products are decomposed above 4.0 V in which carbon and electrolyte will also be decomposed. This will induce improved overpotential and shortened cycle life. So that carbon material loading with sufficient bifunctional catalyst is relatively excellent choice because catalyst will lower Li_2O_2 decomposition voltage. Precious metal[10], metal oxide[11], metal sulfide[12], metal nitride[13] are deeply investigated as Lithium-oxygen cathode electrocatalyst. Among them, binary metal oxide[14-18] shows great potential because single metal oxide can only play a role in accelerating one of oxygen reduction reaction (ORR) and oxygen evolution reaction (OER). According to previous research, nanostructure of cathode electrocatalyst is highly related with its performance in lowering overpotential, improving specific capacity and prolonging cycle life. Its intrinsic character of high specific surface area, abundant active sites and better electron conductivity is beneficial to lower ORR and OER overpotential. Porous structure is important for transportation of O_2 and electron, immersion of electrolyte and deposition of discharge products. Uniformly porous binary metal oxide[16] and hierarchical porous carbon material[19-22] have been widely investigated as lithium-oxygen cathode electrocatalyst. In previous researchers' work[23], mesoporous are suggested to be beneficial to Li^+ , O_2 diffusion and macropores are suggested to provide space for Li_2O_2 deposition. Herein a binary metal oxide with nanotube morphology and hierarchical pore distribution is synthesized with two steps. Its catalysis effect as cathode electrocatalyst in lithium-oxygen batteries is also investigated.

2. EXPERIMENTAL SECTION

2.1 Nickel Cobaltate nanotube synthesis

The material is synthesized according to the literature[24, 25] with little modification. In a typical method, 0.25 g $\text{Ni}(\text{Ac})_2 \cdot 4\text{H}_2\text{O}$ and 0.5 g $\text{Co}(\text{Ac})_2 \cdot 4\text{H}_2\text{O}$ were dissolved into 6 mL of 1,3-isopropanediol. Then 94 mL of isopropanol were added into above solution with stirring for 0.5 h. After that, the mixed solution was transferred into a Teflon-lined stainless steel autoclave and heat-treated at 160 °C for 12 h. After naturally cooling to room temperature, the layered dihydroxide (LDH) precursor was separated by centrifugation, washed with ethanol for three times and dried at 40 °C for 12h. Then the light green precursor was annealed in 300 °C for 2 h and the NiCo_2O_4 black powder was obtained.

2.2 Physical and electrochemical characterization

The crystal structure, morphology, and specific surface area of the as-synthesized samples were examined with powders X-ray diffraction (XRD) (Bruker D8 Advance X-ray diffractometer) with $\text{Cu K}\alpha$ radiation, field-emission scanning electron microscopy (FE-SEM, HitachiS-4800A), transmission electron microscopy (TEM, JEM-2100F) and Brunauer-Emmett-Teller (BET) analysis (Quadratorb SI

Automated Analyser). The cycled electrodes were also analyzed by SEM and Fourier-transform infrared reflection (FTIR) (Shimadzu IRPrestige-21).

The oxygen electrode was prepared as follows: an ink slurry composed of catalyst, super-P and polyvinylidene fluoride (PVDF) with 2:6:2 ratio was stirred and painted onto Celgard 3500 membrane, and dried under vacuum in 80°C for 12h. As a comparison, the super-P mixed with XC-72r electrode was composed of 20 wt% Vulcan XC-72r carbon black, 60 wt% super-P, and 20 wt% PVDF. The super-p electrode was composed of 80 wt% super-P and 20 wt% PVDF. The O₂ electrode was punched into small disks with diameter of 14 mm. The loading on each electrode is about 1.0-1.5 mg, while the specific capacity is calculated on the mass of carbon and the catalyst. The tested battery was assembled by stacking Li foil, electrolyte, O₂ electrode and current collector in a swagelok cell. The electrolyte is composed of 0.5 M lithium bis(trifluoromethanesulfonyl) imide (LiTFSI) in tetraethylene glycol dimethoxyethane (TEGDME). The cell was assembled in an argon-filled glovebox and tested in an O₂ filled glovebox. The galvanostatic charge/discharge measurements were conducted using Land BT2000 test system (Wuhan Land Electronic Co. Ltd. China) between 2.0 V and 4.4 V in different current density. The cyclability was conducted with restricted specific capacity of 500 mAh g⁻¹ until the terminal discharge voltage falls below 2.0 V. Electrochemical impedance spectroscopy (EIS) of the cell at different states were measured on an electrochemical workstation (Zahner IM6e). All of the tests were carried out at room temperature.

3. RESULTS AND DISCUSSION

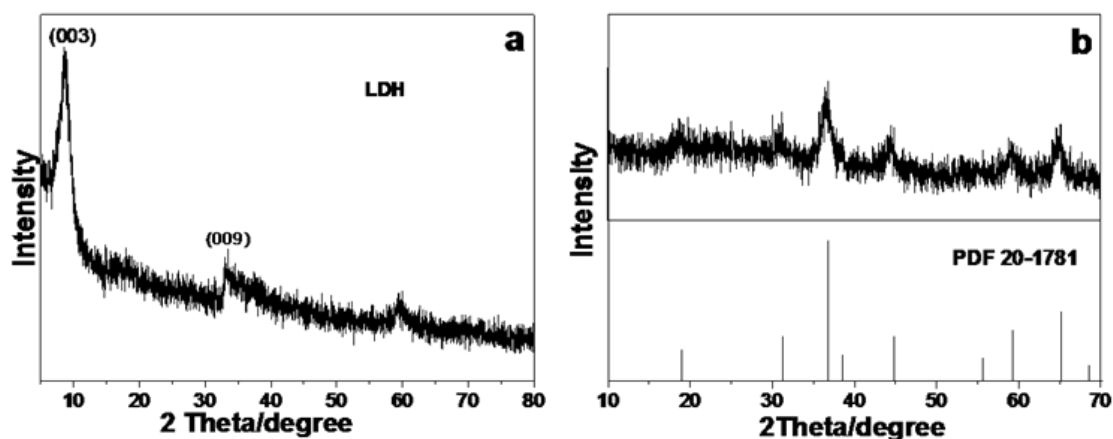


Figure 1. Powder XRD of layered dihydroxide (LDH) precursor and as-synthesized NiCo₂O₄.

Fig. 1a shows the powder XRD pattern of the layered dihydroxide (LDH) precursor. Two diffraction peaks can be assigned to (003) and (009) lattice planes, indicating the precursor is of 2D dimensional layered structure. XRD patterns showed in Fig. 1b are consistent with PDF card (20-1781), indicating cubic NiCo₂O₄ is formed after annealing. Evolution of CO₂ and H₂O will produce various pores in the maintained nanoflake structure. Fig. 2a shows a typical type-III adsorption-

desorption isotherms with H3 loop. It suggests the pores are mainly uniform mesoporous. The flake-like subunits also aggregate forming macropores. BET specific surface area of the sample is measured to be $123.09 \text{ m}^2 \text{ g}^{-1}$. In Fig. 2b, pore size is calculated to be around 4 nm and 6 nm according to Barrett, Joyner and Halenda (BJH) method. These mesoporous are mainly produced by the removal of CO_2 and H_2O and the structural contractions accompanied with the decomposition of the precursors[24].

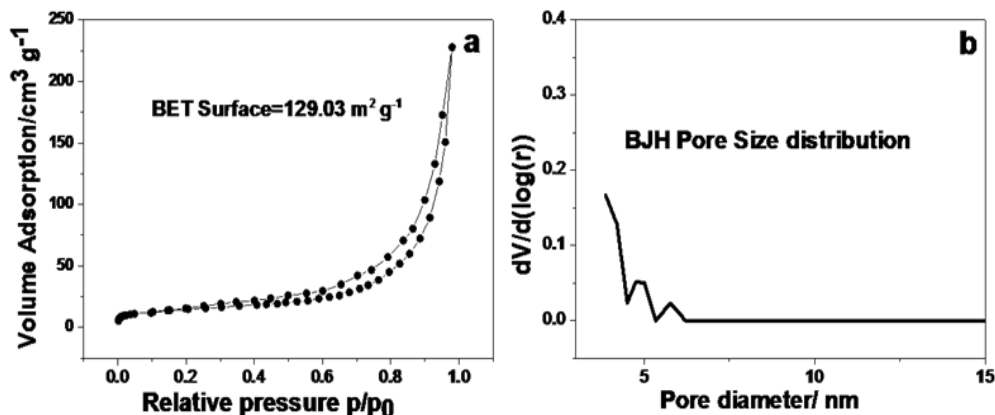


Figure 2. N_2 adsorption-desorption isotherms (a) and BJH pore size distribution (b) of as-prepared NiCo_2O_4 samples.

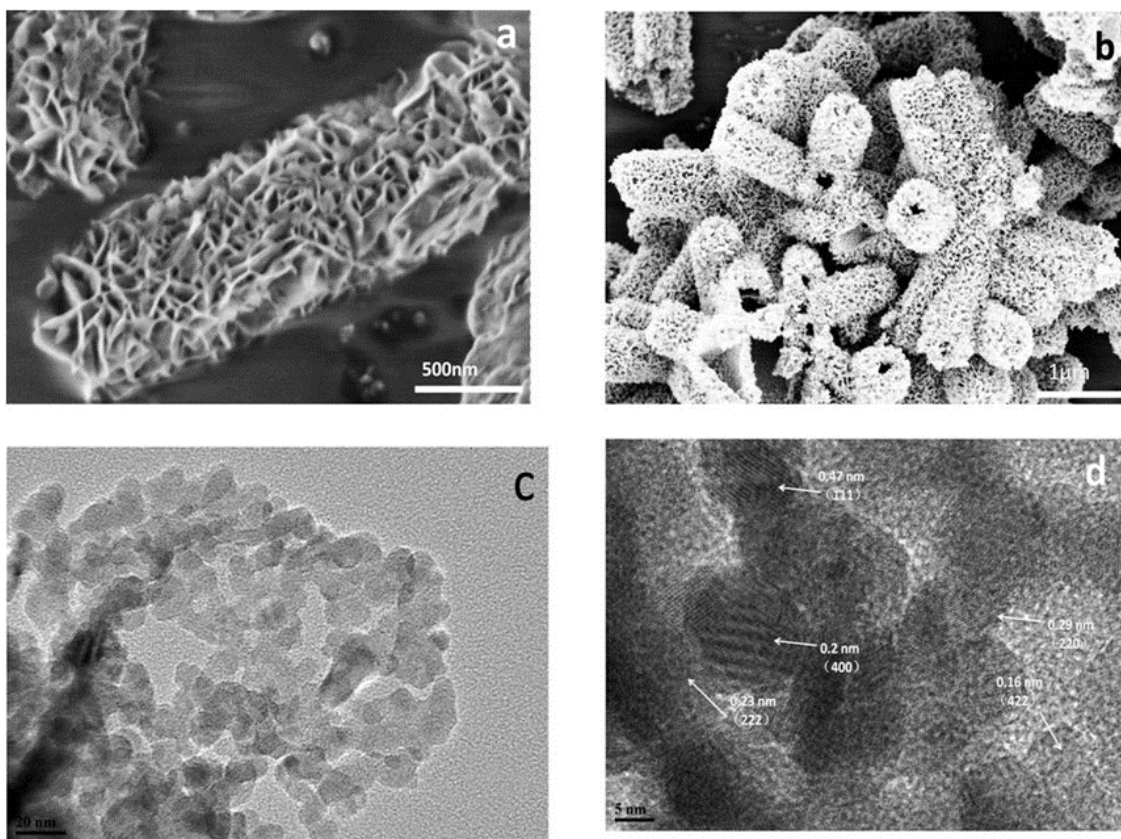


Figure 3. SEM images of the LDH precursor (a) and NiCo_2O_4 (b) at different magnification. High-resolution TEM images (c) and lattice fringe (d) of NiCo_2O_4 samples.

In SEM images (Fig. 3a), the LDH precursors show a morphology of nanotube comprised of nanoflakes. Diameter and length of the nanotube is about 500 nm and 1.5 μm respectively. After annealing, Fig. 3b shows the nanotube structure is maintained with integrity while the dimension is about 400 nm and 1.5 μm respectively. Fig. 3c shows a typical subunit of the nanotube, which is also composed of small crystal powders. Mesoporous ranging from 2 to 5 nm are distributed in the nanosheet randomly, which is in agreement with the BET results. In Fig. 3d, the spacing of adjacent fringe of lattice is 0.47 nm, 0.29 nm, 0.23 nm, 0.2 nm, 0.16 nm, corresponding to (111), (220), (222), (400), (422) crystal spacing of cubic NiCo_2O_4 crystal.

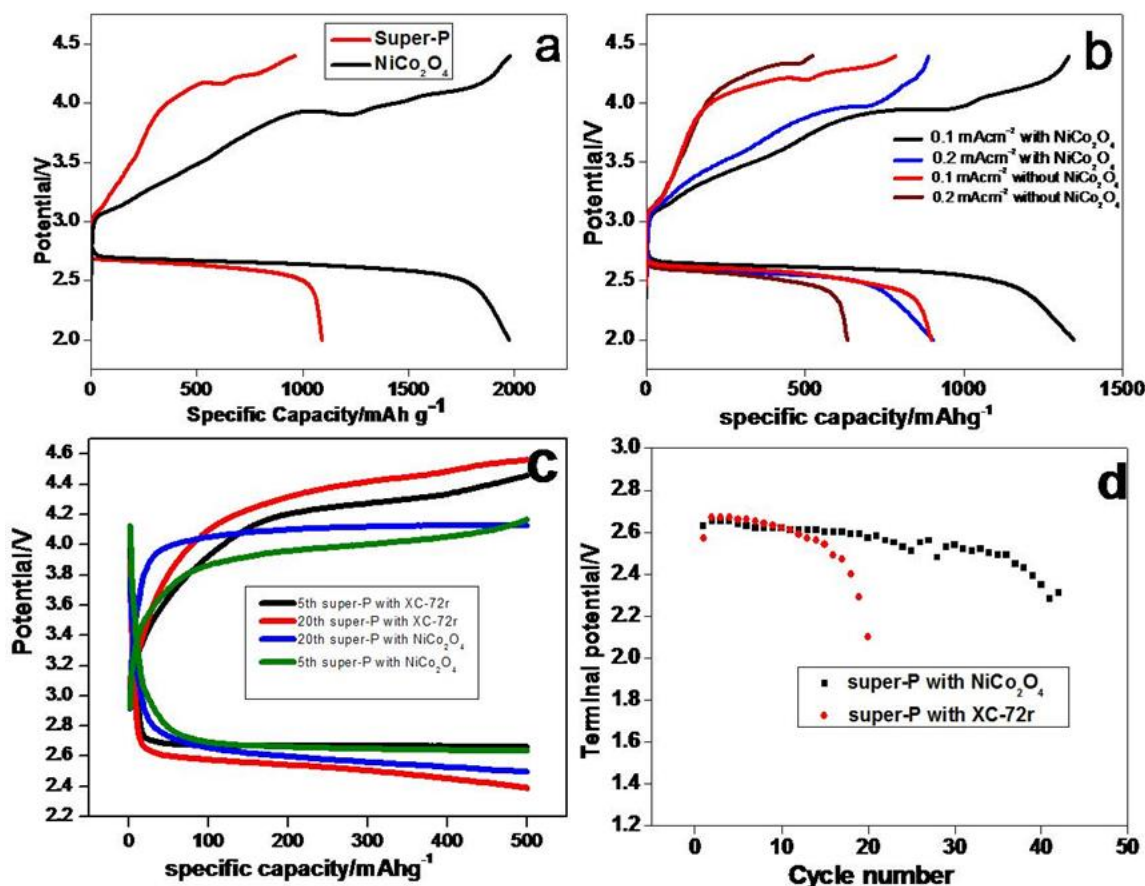


Figure 4. First discharge-charge profiles of the cell with/without NiCo_2O_4 as catalyst (a), Rate performance of the NiCo_2O_4 -based cell and super-P-based cell (b), Cycle performance of the NiCo_2O_4 -based cell and carbon-based cell with a limited specific capacity of 500 mAh g^{-1} (c) and the terminal discharge potential of NiCo_2O_4 -based cell and carbon-based cell (d).

Galvanostatic charge/discharge measurements were conducted to intercept the catalysis function of the catalyst in lithium-oxygen battery. At current density of 0.05 mA cm^{-2} , the first-cycle discharge and charge specific capacities of NiCo_2O_4 -based battery are $1979.4 \text{ mAh g}^{-1}$ and $1976.8 \text{ mAh g}^{-1}$ respectively, which are both prolonged evidently compared to super-P based battery (Fig. 4a). Besides extended specific capacity, the average voltage of the charge reaction (OER) is evidently reduced from 4.14 V to 3.92 V, indicating the excellent OER catalysis activity of the NiCo_2O_4 catalyst.

Apparently most discharge products are decomposed below 4.0 V. In Fig. 4b, with the increase of the current density, both discharge and charge specific capacity decreased. At current density of 0.1 mA cm^{-2} and 0.2 mA cm^{-2} , the discharge specific capacity is 1346 mAh g^{-1} and 901 mAh g^{-1} . Notably, average voltage of charge decreased with the increase of the discharge current density. This phenomenon was because that smaller Li_2O_2 powders were generated at higher current density, which can be decomposed in relatively lower voltage[26].

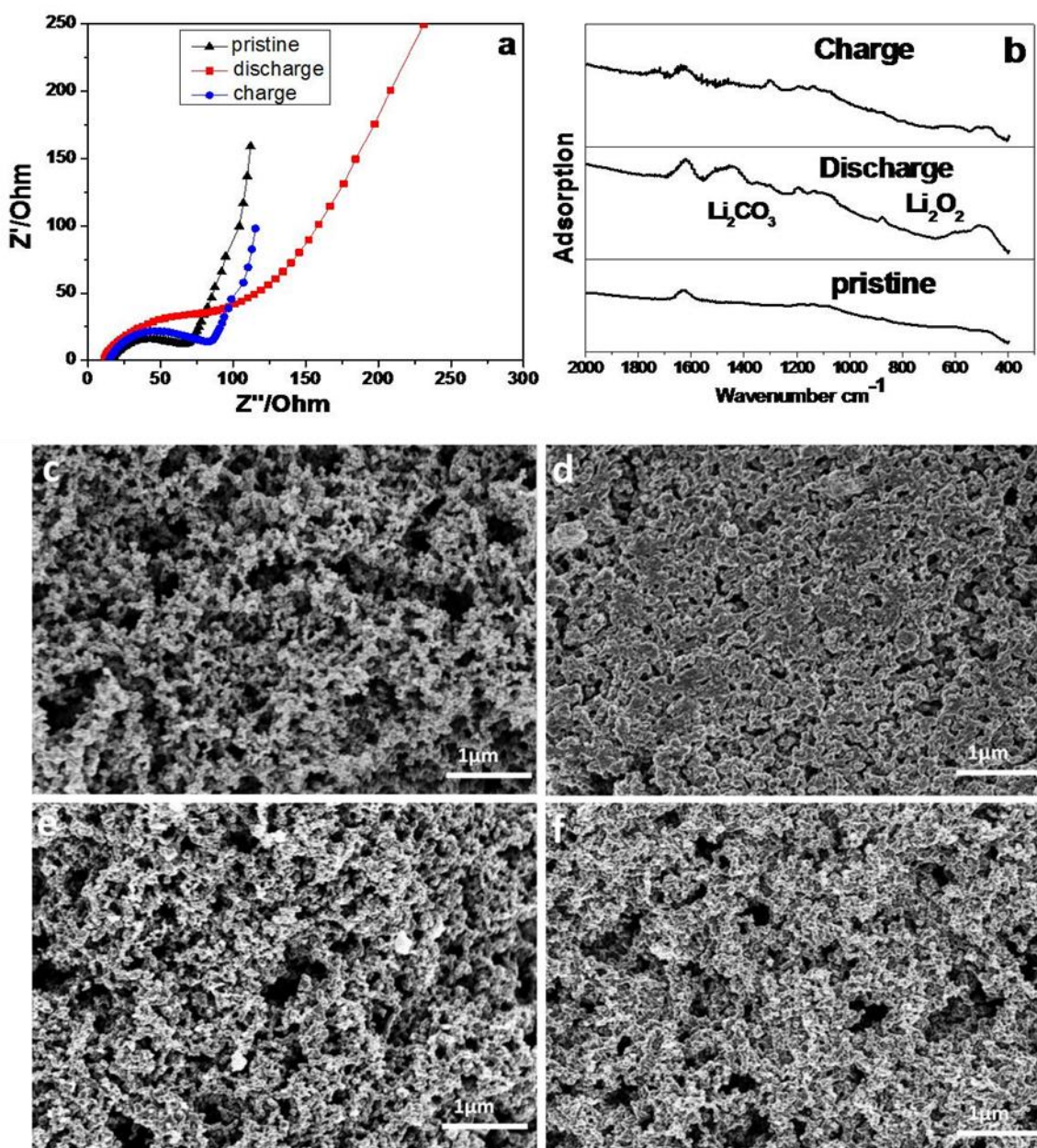


Figure 5. (a) Electrochemical impedance spectroscopy (EIS) of the cells at different stages. (b) FTIR spectra of the electrode at different stages in the first cycle. SEM images of the electrode surface at different stages: (c) pristine, (d) after 1st discharge, (e) after 1st charge, (f) after 20th recharge.

The cycle performance is conducted at current density of 0.05 mAh g^{-1} with limited specific capacity of 500 mAh g^{-1} . The test will end when discharge terminal potential get below 2.0 V. Because super-P-based cell can only cycle for 10 cycles with a sudden violent increase of overpotential, a super-p mixed with XC-72r electrode is used as comparison in cycle life test. In Fig. 4c, NiCo_2O_4 -based cell showed much decreased charge overpotential than carbon-based cell in 5th cycle and 20th cycle. The NiCo_2O_4 -based battery can run for 42 cycles before its discharge terminal potential dropped below 2.0 V, while carbon-based battery can only run for 20 cycles.

Electrochemical impedance spectroscopy (EIS) was used to study the resistance variation of the cell under different stages. An intermediate frequency semicircle and a low frequency tail were observed in Fig. 5a. The intermediate frequency semicircle represents charge transfer resistance (R_{ct}) so that it can reflect the amount of deposition in the cathode. R_{ct} after recharge is smaller than R_{ct} after discharge and still larger than R_{ct} before discharge. Products (Li_2CO_3 and LiRCO_3 (R=alkyl)) that can't be decomposed by charge should be responsible for this increase[27]. FTIR spectrogram of electrode was used to intercept the discharge products and reversibility of the cell. In Fig. 5b, Li_2CO_3 and Li_2O_2 are both detected in cathode after discharge, though their characteristic adsorption peaks disappear after recharge. Because Li_2CO_3 will not be decomposed in charge[28], it is assumed to be product of Li_2O_2 with CO_2 in air. Fig. 5c, d, e, f show the SEM images of the electrode surface at different stages. Before 1st discharge, super P and the catalyst are dispersed uniformly and homogeneously on the cathode, forming a number of accumulated pores. After 1st full discharge, the film-like discharge products grow along the electrode surface and completely cover the holes. However, after charge, the holes and electrode surface are recovered with the decomposition of the discharge products. As we can see in Fig. 5f, discharge products can still be mostly decomposed even after 20th cycles. This results show the excellent reversibility of the cell with NiCo_2O_4 nanotube as cathode electrocatalyst.

4. CONCLUSION

In summary, NiCo_2O_4 nanotube consisted of nanoflakes was synthesized with hydrothermal reaction and following annealing. The specific morphology, hierarchical pores and binary metal synergistic effects of NiCo_2O_4 nanotube make the lithium-oxygen batteries used NiCo_2O_4 -based electrodes exhibit improved battery performance, such as evidently improved energy efficiency (2.64/3.92 V), specific capacity (1979 mAh g^{-1}) and cycle life (44 cycles).

ACKNOWLEDGEMENTS

The authors acknowledge funding support from 973 program (2014CB932301), Natural Science Foundation of China (No. 21471034), the National Natural Science Foundation (No. 21473040) and Science & Technology Commission of Shanghai Municipality (No. 08DZ2270500), China.

References

1. K. M. Abraham and Z. Jiang, *J. Electrochem. Soc.*, 143 (1996) 1.
2. Z. Y. Lyu, Y. Zhou, W. R. Dai, X. H. Cui, M. Lai, L. Wang, F. W. Huo, W. Huang, Z. Hu and W. Chen, *Chem. Soc. Rev.*, 46 (2017) 6046.

3. C. Liu, W. R. Brant, R. Younesi, Y. Dong, K. Edstrom, T. Gustafsson and J. Zhu, *ChemSusChem*, (2017) DOI: 10.1002/cssc.201601718.
4. Z. Ma, X. Yuan, L. Li, Z.-F. Ma, D. P. Wilkinson, L. Zhang and J. Zhang, *Energy Environ. Sci.*, 8 (2015) 2144.
5. A. Arul, H. Pak, K. U. Moon, M. Christy, M. Y. Oh and K. S. Nahm, *Appl. Catal. B-Environ.*, 220 (2018) 488.
6. J. Xiao, D. Mei, X. Li, W. Xu, D. Wang, G. L. Graff, W. D. Bennett, Z. Nie, L. V. Saraf, I. A. Aksay, J. Liu and J. G. Zhang, *Nano lett.*, 11 (2011) 5071.
7. T. Zhang and H. Zhou, *Angew. Chemie*, 51 (2012) 11062.
8. R. R. Mitchell, B. M. Gallant, C. V. Thompson and Y. Shao-Horn, *Energy Environ. Sci.*, 4 (2011) 2952.
9. X. Lin, L. Zhou, T. Huang and A. Yu, *J. Mater. Chem. A*, 1 (2013) 1239.
10. Z. Peng, S. A. Freunberger, Y. Chen and P. G. Bruce, *Science*, 337 (2012) 563.
11. Q. Liu, Y. Jiang, J. Xu, D. Xu, Z. Chang, Y. Yin, W. Liu and X. Zhang, *Nano Res.*, 8 (2014) 576.
12. M. Asadi, B. Kumar, C. Liu, P. Phillips, P. Yasaei, A. Behranginia, P. Zapol, R. F. Klie, L. A. Curtiss and A. Salehi-Khojin, *ACS nano*, 10 (2016) 2167.
13. J. Park, Y. S. Jun, W. R. Lee, J. A. Gerbec, K. A. See and G. D. Stucky, *Chem. Mater.*, 25 (2013) 3779.
14. H. S. Jadhav, R. S. Kalubarme, A. H. Jadhav and J. G. Seo, *J. Alloys Compd*, 666 (2016) 476.
15. J. G. Kim, Y. Kim, Y. Noh and W. B. Kim, *ChemSusChem*, 8 (2015) 1752.
16. Y. Li, L. Zou, J. Li, K. Guo, X. Dong, X. Li, X. Xue, H. Zhang and H. Yang, *Electrochim. Acta*, 129 (2014) 14.
17. L. Wang, X. Cui, L. Gong, Z. Lyu, Y. Zhou, W. Dong, J. Liu, M. Lai, F. Huo, W. Huang, M. Lin and W. Chen, *Nanoscale*, 9 (2017) 3898.
18. H. Wu, W. Sun, Y. Wang, F. Wang, J. Liu, X. Yue, Z. Wang, J. Qiao, D. W. Rooney and K. Sun, *ACS Appl. Mater. Inter.*, 9 (2017) 12355.
19. W. Zhou, H. Zhang, H. Nie, Y. Ma, Y. Zhang and H. Zhang, *ACS Appl. Mater. interfaces*, 7 (2015) 3389.
20. J. Li, Y. Zhang, W. Zhou, H. Nie and H. Zhang, *J. Power Sources*, 262 (2014) 29.
21. M. J. Song, I. T. Kim, Y. B. Kim, J. Kim and M. W. Shin, *Electrochim. Acta*, 230 (2017) 73.
22. Y. Lin, B. Moitoso, C. Martinez-Martinez, E. D. Walsh, S. D. Lacey, J. W. Kim, L. Dai, L. Hu and J. W. Connell, *Nano Lett.*, (2017) DOI: 10.1021/acs.nanolett.7b00872.
23. Z. Guo, D. Zhou, X. Dong, Z. Qiu, Y. Wang and Y. Xia, *Adv. Mater.*, 25 (2013) 5668.
24. F. X. Ma, L. Yu, C. Y. Xu and X. W. Lou, *Energy Environ. Sci.*, 9 (2016) 862.
25. B. Sun, X. Huang, S. Chen, Y. Zhao, J. Zhang, P. Munroe and G. Wang, *J. Mater. Chem. A*, 2 (2014) 12053.
26. H. Lee, Y.-J. Kim, D. J. Lee, J. Song, Y. M. Lee, H.-T. Kim and J.-K. Park, *J. Mater. Chem. A*, 2 (2014) 11891.
27. L. Ye, W. Lv, J. Cui, Y. Liang, P. Wu, X. Wang, H. He, S. Lin, W. Wang, J. H. Dickerson and W. He, *ChemElectroChem*, 2 (2015) 312.
28. M. Hong, H. C. Choi and H. R. Byon, *Chem. Mater.*, 27 (2015) 2234.